Ceramics-Silikáty 64 (2), 227-238 (2020)
www.ceramics-silikaty.cz doi: 10.13168/cs.2020.0012

STRENGTHS OF SULFOALUMINATE CEMENT CONCRETE AND ORDINARY PORTLAND CEMENT CONCRETE AFTER EXPOSURE TO HIGH TEMPERATURES

JEAN JACQUES KOUADJO TCHEKWAGEP, SHOUDE WANG, ANOL K. MUKHOPADHYAY, #SHIFENG HUANG, XIN CHENG

Shandong Provincial Key Laboratory of Preparation and Measurement of Building Materials, University of Jinan, Shandong 250022, China

#E-mail: mse_huangsf@ujn.edu.cn

Submitted October 25, 2019; accepted January 3, 2020

Keywords: Sulfoaluminate cement, Flexural strength, Cracking load, High temperatures, Porosity

The use of SAC (sulfoaluminate cement) has been increasing in the constructions of diverse buildings with some close to reactors, which are often exposed to high temperatures in China. This study compares the flexural strength, compressive strength, crack load, mass weight loss, porosity, and flexural stress--strain of the sulfoaluminate cement concrete (SACC) to that of ordinary Portland cement concrete (OPCC) after both are exposed to high temperatures. The results show that the samples of SACC show a rapid decrease in the flexural strength, crack load, and compressive strength after heating, and, thus, cannot be repaired, but should be demolished. Samples made with OPCC can be repaired because the structural integrity remains acceptable after heating. 56 % SACC is < half of its initial strength after heating to 200 °C while OPCC remains at > 90 % of its compressive strength after heating at 200 °C, and retains 80 % of its compressive strength when heated to 300 °C. SACC initially had a higher flexural strength and consequently a higher crack load; therefore, it performed better than the OPCC in terms of the load carrying capacity of the structure. Also, the OPCC had a constant decrease in the strength, compared to the SACC which did not. However, the OPCC has a better resilience strength rating as the temperatures increase than the SACC one because testing revealed a very rapid decrease in the strength after exposure to 100 °C, 200 °C, and 300 °C. The results agree on the better firm structure uniformity and density of the SACC at an ambient temperature (20 °C) compared to the OPCC. The severe deterioration (micro-crack) inside both concretes, revealed by the longer transmitting time and the small amplitude values of the waves, indicated the effective negative impact which is no longer demonstrated when the extreme temperature has a larger effect on the concrete made with SAC, therefore, the other results highlighted the rapid decrease in the strength of the SACC compared to that of the OPCC.

INTRODUCTION

Rapid sulfoaluminate cement is widely used in China and abroad because of its early strength, high strength, frost resistance, impermeability, corrosion resistance, and low alkalinity [1]. It also takes less energy to produce than other types of cement. Ordinary Portland cement (OPC) and the rapid sulfoaluminate cement (SAC) are widely used around the world [2, 3]. SACC has represented an important area of research in material science since its discovery in the 1970s in China [4, 5, and 6]. The purpose of this study is to investigate and characterise SACC and the OPCC after exposure to high temperatures. The results could contribute to the technical parameter data, and could help those involved in damage estimation and the repair of structures made with SACC. It would also provide a reference for deterioration estimation and a maintenance aid after high temperature exposure to structures made with SAC. In this study, samples of SACC and OPCC were cast and allowed to cure for 28 days. The samples were then exposed to high temperatures, allowed to cool for 7 days and then tested for the following properties: Mass weight loss after heating and cooling, cracking load, flexural strength, flexural stress-strain, compressive strength and porosity. We also recorded and characterised the ultrasonic sound waves before and after heating for 28 days for SACC and OPCC. This research paper focused on investigating, analysing and comparing the parameters of the different mechanical properties mentioned above and exploiting ultrasonic waves (UW) testing data to understand the homogeneity and density of the different samples before and after being exposed to different temperatures.

Aim

- Compare the SACC and OPCC flexural strength, cracking load and compressive strength
- Observe and characterise the flexural stress-strain of SACC and OPCC
- Observe and characterise the transmission of ultrasonic waves through SACC and the OPCC before and after heating.
- Use porosity testing to validate the interpretations of the changes in strength in terms of the microstructural modifications after exposure to high temperatures for both concretes for rebuilding purposes.

Table 1. The SAC full analysis – Vac 28 mm of the sulfoaluminate cement used (KCps).

CaO	Al_2O_3	SO_3	SiO_2	Fe_2O_3	MgO	TiO_2	K_2O	SrO	Na_2O	Cl	P_2O_5
519.4	86.2	86.2	40.5	80.0	13.1	5.1	6.8	59.9	0.5	1.3	0.5
45.28 %	17.51 %	15.76 %	9.19 %	2.50 %	1.90 %	0.75 %	0.48 %	0.17 %	0.19 %	0.11 %	0.10 %

EXPERIMENTAL

Material used and proportions

Rapid SAC – 42.5 and OPC with 42.5 grade strength, both with a specific gravity of 3.14, were used with the chemical compositions shown in Table 1 and 2. A coarse agglomerate with a nominal scale maximum size between 5 to 25 mm and river quartz sand as the fine aggregate with a size of 0.6 to 4.75 mm were utilised as the constituents. The specific gravity of fine aggregate and coarse aggregate is 2.7 and 2.68, respectively. The aggregate gradations are shown in Table 3. The concrete blend was designed and subjected to a test according the Chinese standard experimental test method regulations GB50081-2002 for the mechanical properties of ordinary concrete [7, 8]. The different mix design propositions are shown in Table 4. The workability was improved by adding a chemical retardant polycarboxylate superplasticizer since the cement (R.SAC-42.5) used mostly sets quickly, the dosage was calculated based on the cement volume.

Table 2. The OPC chemical composition of the cement (wt. %).

SiO_2	Al_2O_3	Fe_2O_3	CaO	MgO	SO_3	Cl
21.45	5.93	3.45	60.87	3.12	2.35	0.027

Table 3. The aggregate gradation.

Limestone (5-25 mm)		Quartz sand (0.6 - 4.75 mm)	
Sieve size	% retained	Sieve size	% retained
Gradation		Gradation	
0 ~ 5	5 %	0 ~ 0.6	20 %
5 ~ 10	25 %	0.6 ~ 1.18	45 %
10 ~ 15	50 %	1.18 ~ 2.36	25 %
15 ~ 20	15 %	2.36 ~ 4.75	10 %
20 ~ 25	5 %	–	–

Table 4. The sulfoaluminate cement concrete and the ordinary Portland cement concrete mix proportions.

`	SACC unit weight (per m^3)	OPCC unit weight (per m^3)
Cement	430	430
Water	160	160
Gravel 5 - 25	975	975
Quartz sand 1.6 - 2.6	835	835
Retarder	4.3	4.3
w/c	0.4	0.4

Experimental set-up and test programme

The SACC and OPCC samples with a size of 400 × 100 × 100 mm (27 samples) for the flexural strength test and 100 × 100 × 100 mm (27 samples) for the compressive strength test were cast and cured in the chambers of the material testing cure room with a temperature range of ± 20 °C [9] and were demoulded after 28 days. Afterwards, they were air-dried for 5 days in the laboratory, then each sample was exposed to 100 °C, 200 °C and 300 °C for 4 hours for testing, see Figure 1. This exposure time was found to be adequate for the complete dehydration of the important mineral ingredients for the SAC: the AFt (ettringite) and $Al(OH)_3$ solid crystal which make up 40 - 70 wt. % and are the most abundant and the most important minerals that make the cement and assure the bonding with different aggregates [10, 11, 12] as well as other related dehydration reactions and other thermally induced physical changes [13, 14]. Each sample was allowed to cool down for seven days for observing the capacity of the different cements (SAC and OPC) to recover the strength lost after being exposure to 100 °C, 200 °C and 300 °C. The samples were then equipped on their surface with a BQ120-80AA resistance 120.3 ± 0.1 gauge factor 2.20 ± 1 % lot no.1901.01×12W4SB grade "A" from China AVIC Electric Instrument Co., Ltd. [15, 16] as shown in Figure 2 to separately record with the aid of the DH3818Y static strain tester [17, 18] the flexural stress-strain of each sample during the flexural testing

Figure 1. The arrangement of the samples inside the high temperature electric furnace.

application loads as shown in Figure 3. The ultimate testing machine (UTM) with an adequate capacity and with a layer of two steel skates of 38 mm was used, on which, the concrete samples were supported. The skates were assembled with a distance from centre to centre of 20 cm. Each sample was cautiously seated on the machine as shown in Figure 3a by positioning the centre of the specimen and the two-point load applied to the samples in the manner that the load was cast in the mould. The load exercised was in the range of 0.05 MPa·s^{-1}

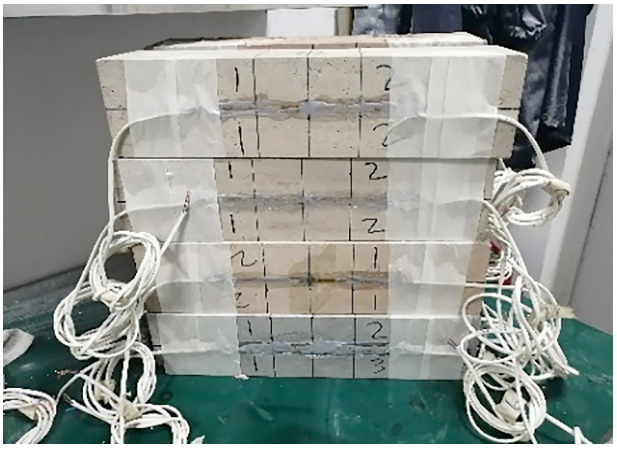

Figure 2. The sample equipped on the surface with a sensor strain gauge able to record the flexural stress-strain in the concrete.

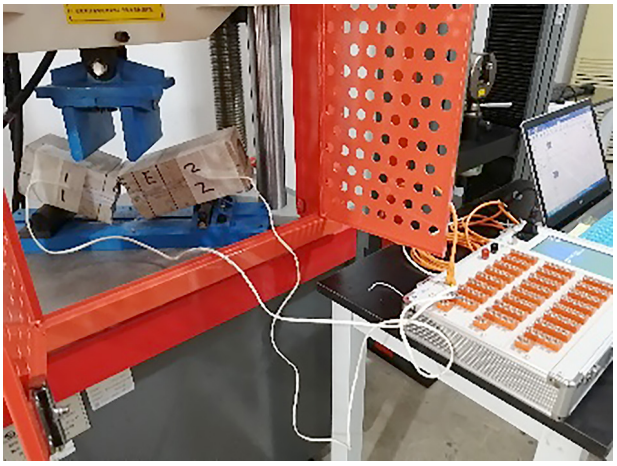

a) The ultimate testing machine (UTM)

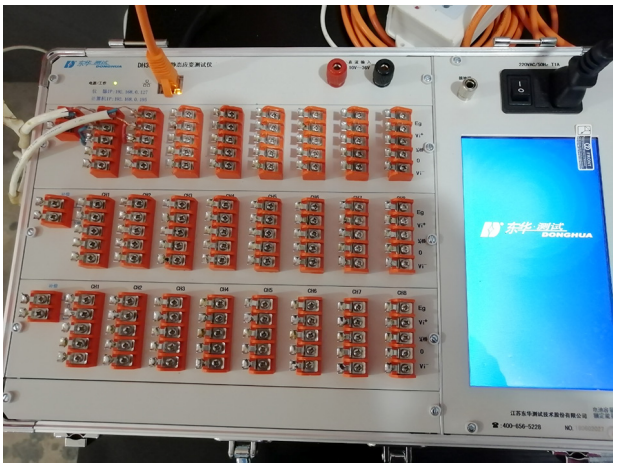

b) DH3818Y static strain tester

Figure 3. The experimental device.

Figure 4. The ultrasonic instrument.

a) The samples before heating

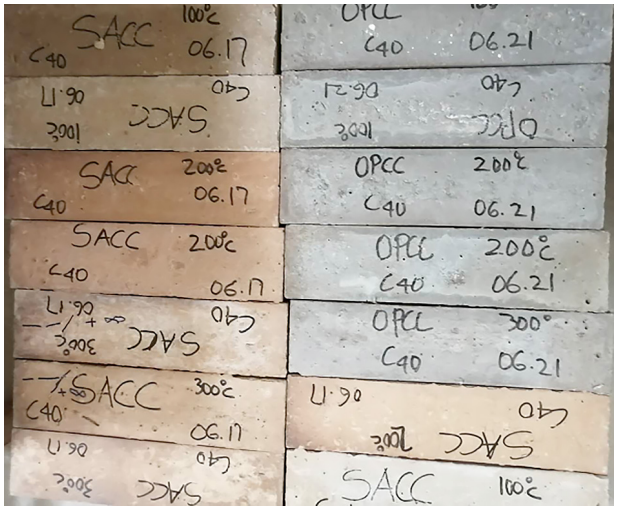

b) The samples after heating at the different temperatures

Figure 5. The treatment set-up on the samples. *(Continue on next page)*

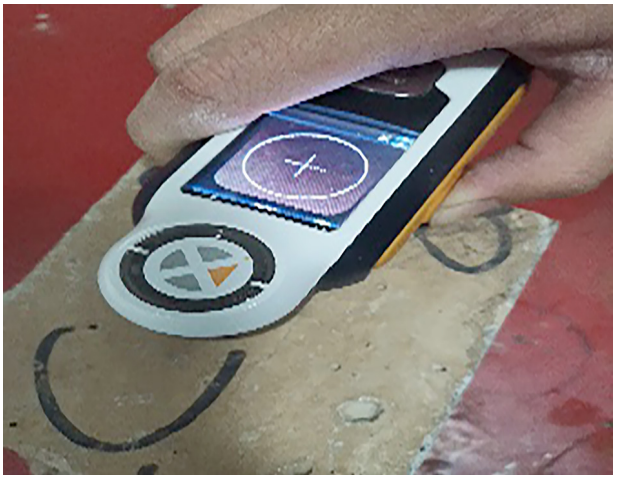

c) The colorimeter Instrument RM200QC testing

Figure 5. The treatment set-up on the samples.

without moving and progressively increased until the sample breaks and the crack load is recorded.

A Tektronix AFG3022B arbitrary waveform generator and a Tektronix TDS1002B-SC were the source and receiver of the digital oscilloscope signal used in this experiment [19, 20], respectively. The ultrasonic wave's frequency was 50 KHz and the input voltage was 10 V. The transmitting amplitude values, times, and waveform of the ultrasound were recorded. An ultrasonic wave (UW) test was performed on the samples before and after heating, as shown in Figure 4. The change in the ultrasonic wave can reflect the internal element before the heat, then show the internal degradation of the concrete sample after the heat, therefore, indicating the internal change in the sample and predicting its failure [21, 22] .

Residual heating electric furnaces are among one of the good heating method options for testing the fire durability of concrete [23, 24]. Figure 5 shows the appearance of the sample before and after heating, which changed more in colour for the SACC. Based on the colorimeter Instrument model RM200QC at the same location on the samples, the colour difference of the heat-treated samples compared to the untreated sample was 19.6 for the SACC and only 5.8 for the OPCC, it became yellowish for the SACC.

RESULTS AND DISCUSSION

Impact of the heat characterised by ultrasonic analysis

When both concretes (SACC and OPCC) have internal cracks (micro-cracks) generated by the heat, the severity of the internal micro-crack can be expressed by the amplitude value, the transmitting time, and waveform changes of the ultrasonic wave [25, 26]. Figure 5 shows typical ultrasonic waveforms for the control sample tested at 20 °C, then 100 °C, 200 °C, and 300 °C obtained before (Figures 6a and e) and after being heated for 4 hours [Figures 6b, c, d and f, g, h) for the SACC and the OPCC, respectively. The transmitting time and amplitude values are acquired from the head wave of the ultrasonic waveform. The average transmitting times before heating for the control samples at 20 °C were 301.51 μs for the SACC and 304.58 μs for the OPCC, and the amplitude average values were 2.38 mV for the SACC and 2.28 mv for the OPCC. When samples were cracked through heating (negative impact), there was a strong interference with the propagation of the ultrasonic wave, which led to an ultrasonic wave with a large transmitting time, small amplitude values, and unstable waveform. After heating at different temperatures, the transmitting times of the samples at 100 °C, 200 °C and 300 °C were increased to 376.57 μs, 407.31 μs, and 313.84 μs for the SACC and 414.06 μs, 324.75 μs and 329.42 μs for OPCC, and the amplitudes values decreased to 0.96 mV, 0.82 mV, and 0.81 mV and 1.28 mV, 1.20 mV, 0.60 mV respectively for the SACC and the OPCC.

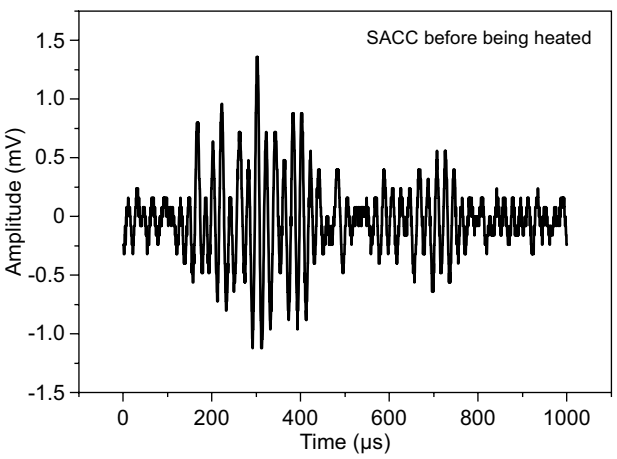

a) 0 °C

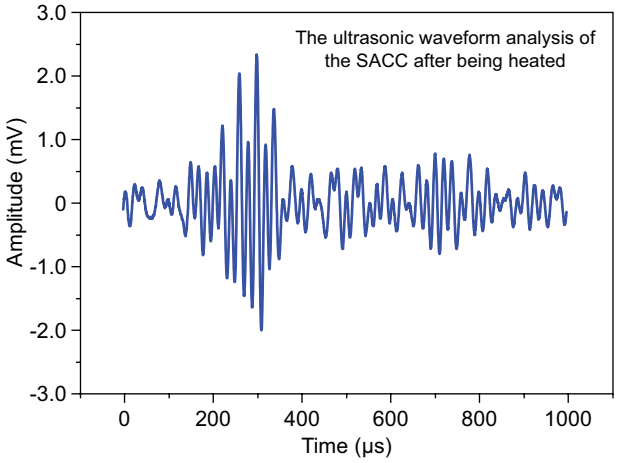

b) 100 °C

Figure 6. The ultrasonic waveform analysis before and after being heated. *(Continue on next page)*

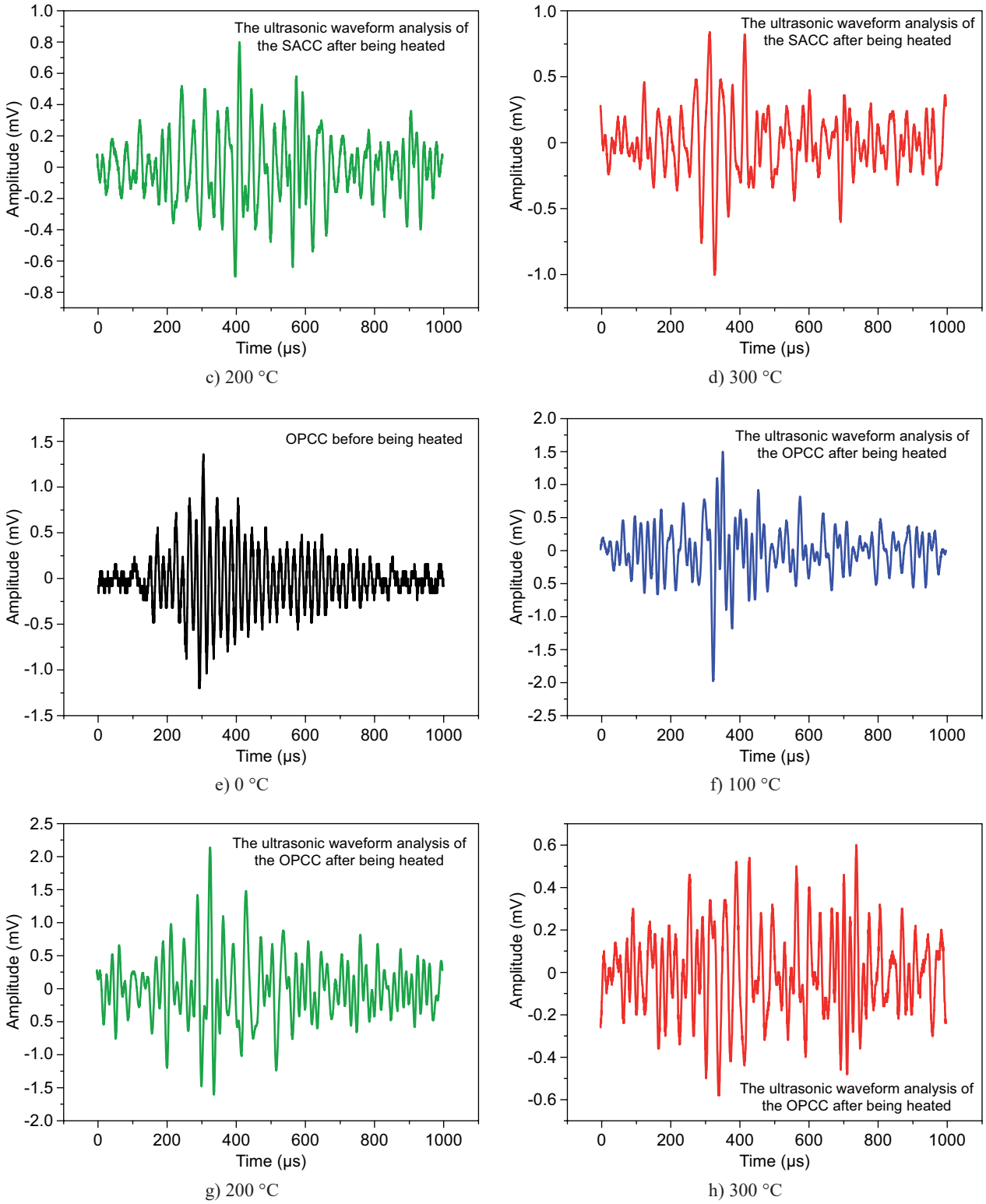

Figure 6. The ultrasonic waveform analysis before and after being heated.

The transmitting times of the ultrasonic waves increased while the amplitude values decreased. The samples tested at the normal temperature (20 °C) for both concretes (SACC and OPCC) have the smallest transmission time and the largest amplitude value, which indicates that the defects inside those samples tested before heating at the different temperatures had a better homogeneity and compactness. After heating, the peak-to-peak variation of those values were less for the SACC (initial value), there is evidence that a more severe effect which the exposure to high temperatures for an extensive period has on the SACC than the OPCC.

Those values were 1.42 mV for 100 °C, 1.56 mV for 200 °C and 1.57 mV for 300 °C against 1 mV for 100 °C, 1.08 mV for 200 °C and 1.68 mV for 300 °C of the initial amplitude value, respectively. The waveform change may be caused by the energy attenuation of the ultrasonic wave during the propagation process which encounters many micro-cracks, see Figure 7. The ultrasonic wave encounters multiple reflections at the concrete interface leading to the waveform attenuation and causing the non-reflecting waves to be observed when the samples are heated.

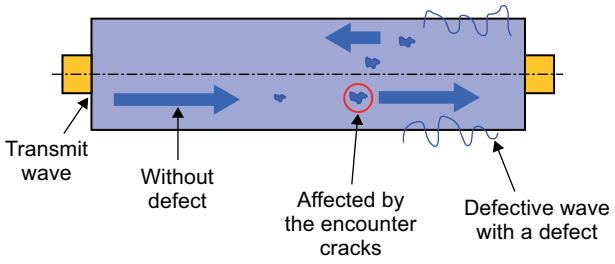

Figure 7. The ultrasonic wave propagates through the concrete sample.

The defects inside the heated samples increased as the temperature increased and was obviously observed more on the surface of the heated sample at 300 °C for the SACC than the OPCC with the cracks and moisture visible to the eye. The stereo microscopic images shown in Figure 8 as well as the SEM pattern in Figure 9 gave extended information showing an inclined main crack distinctly materialising on the surface of the SACC more

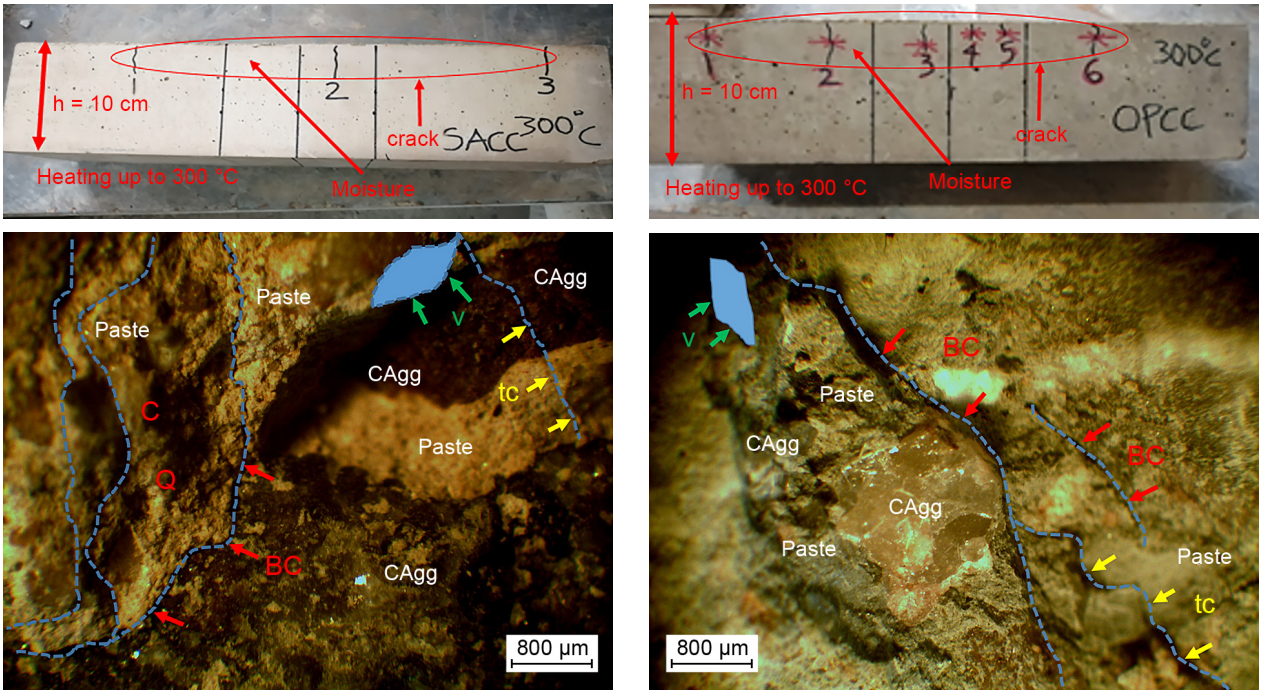

Figure 8. The cracking (left) and moisture (right) appearance and the stereo microscope images of the heat induction micro-cracks in the SACC and OPCC samples immediately after being removed from the furnace exposed at 300 °C for 4 hours, respectively. BC – border crack, V – void, TC – transgranular crack.

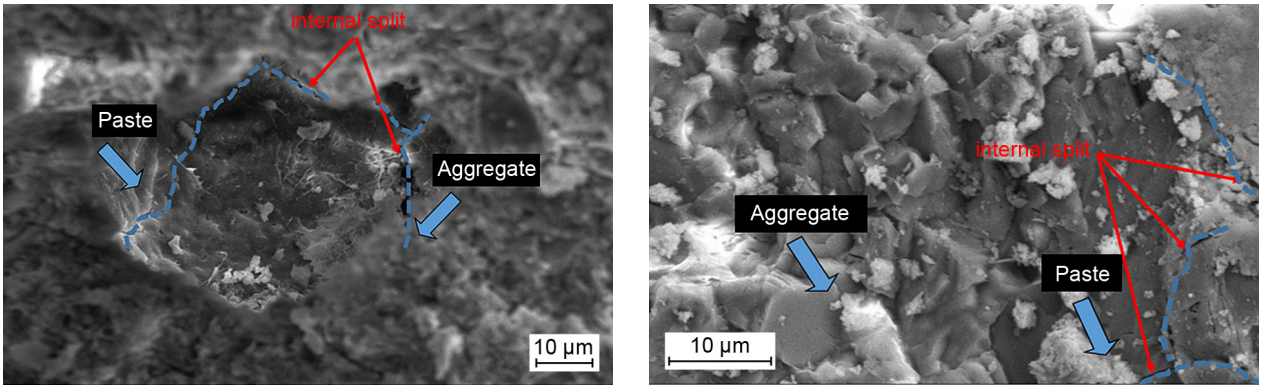

a) SACC b) OPCC

Figure 9. The appearance of the SEM pattern observations of the different levy concrete heated at 300 °C.

than the OPCC. The inclination angle is wide, the crack area is long-drawn-out, and irregular cracks are dispersed on the other parts of the surface.

Flexural performance of the SACC and OPCC

As shown in Figure 10, the SACC mass weight loss is greater, and the weight decreases very rapidly as the temperature increases compared to the OPCC mass weight loss, which decreases as well in a slightly constant tendency as the temperature rises. The loss in mass weight of the samples as the temperature increases is in accordance with the effect of the cement type on the pore pressure and the temperature of the concrete.

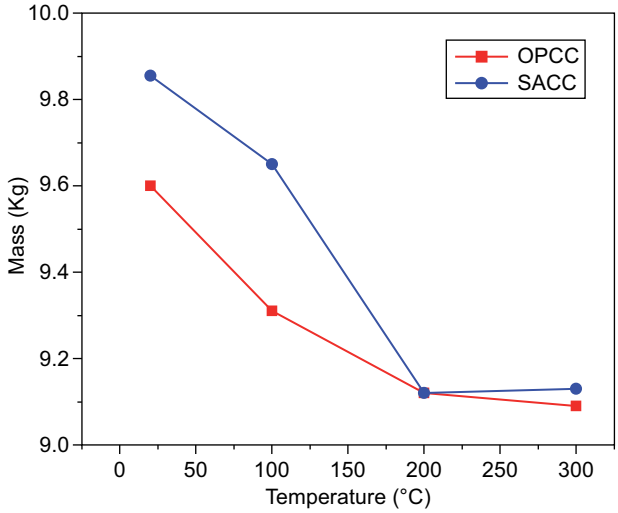

Figure 10. The mass weight loss vs. temperature.

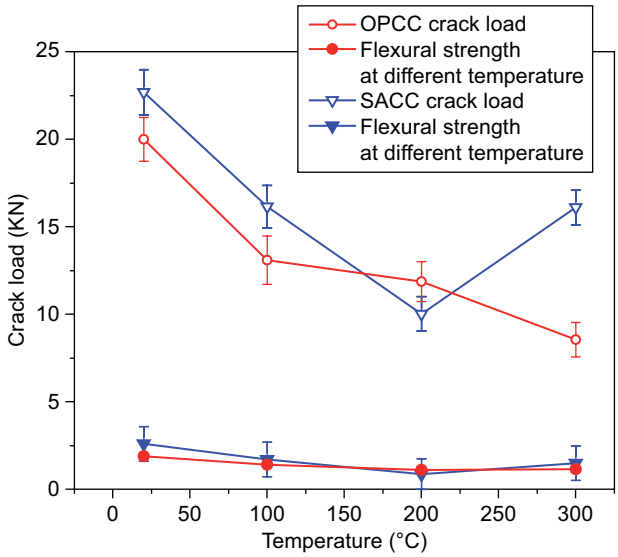

Figure 11. The flexural strength of the SAC and OPC concrete vs. temperature.

The flexural strength overview shows that the SACC is an average 27 % higher than the OPCC for the different temperatures. Its crack load also showed a rapid decrease as the temperature increased, as shown in Figure 11. The crack load as shown in Figure 11 shows that the concrete made with the SAC is initially higher than the one made with the OPC, and, therefore, resists more in flexion after being heated. Nevertheless, the crack load, and, by consequence, the flexural strength, of the SACC decreases rapidly, proof of the more negative influence that the high temperature has on the SAC mineralogy. Which, at around 100 - 200 °C, will experience a lower capillary drainage followed by water damage and the diminution of the cohesion strength as the water increases after the decomposition of the AFt and Al(OH) 3 gel at < 100 °C and ~ 300 °C, the strengthened mineral inside the SAC.

Both concrete samples, after being heated and loaded showed that the decrease in the compressive strength of the SACC rapidly decreased to 55 % of the initial compressive strength at 300 °C against 20 % for the OPCC at 300 °C in the same conditions, as the temperature increased. This is in accordance with the decrease in the strength with the two different cements used. The influence of high temperatures on the compressive strength of the SACC was much more perceptible between 100 to 300 °C, see Figure 12. Under the same temperature range, the OPCC performed much more consistently in decreasing the strength than the SACC.

It is obvious from Table 5 and Figure 11 that the absolute values of the crack load, by consequence of the flexural strength, drastically decreased for the SACC when the temperature increased. This indicates that OPCC is possibly more serviceable than SACC after it has been exposed to 100 °C, 200 °C, and 300 °C. The OPCC lost strength more consistently in the same conditions when compared with the SACC.

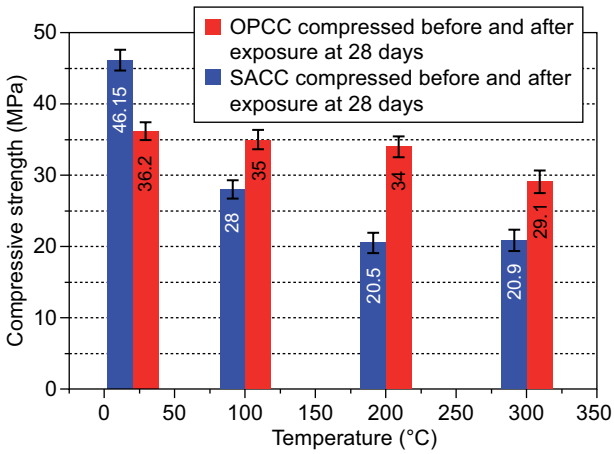

Figure 12. The compressive strengths of the SAC and OPC concrete vs. temperature.

Table 5. The mechanical properties of the different concretes.

Type of concrete `	SACC				OPCC			
Strength grade	C40							
Temperature [°C]	20	100	200	300	20	100	200	300
Flexural strength [MPa]	2.60	1.70	0.87	2.16	1.89	1.40	1.10	1.15
Compressive strength [MPa]	46.15	28	20.5	20.9	36.2	35	34	29.1
Mass [kg]	9.85	9.65	9.12	9.13	9.6	9.31	9.12	9.09

Flexural stress-strain

At 20 °C, the characteristics show a linear elastic behaviour of both concretes (SACC and OPCC) followed by the plastic deformation before reaching the peak stress prior to failure. The elastic behaviour slope followed by a gradual decrease in the slope till it fails (similar to the viscoelastic behaviour) is the characteristic trend from 100 to 300 °C. However, for the OPCC, a much lower trend in the slope is observed as the temperature increased (i.e., a smaller change in the strain with a smaller change in the stress, more viscoelastic and plastic in nature) with a lower decrease in the slope till it fails. The trend in the flexural strain of the SACC and the OPCC indicates that strain varied greatly for the SACC, see Figure 13a. The flexural strain of the SACC and OPCC decreased as the heating temperature increased on both samples confirming the fragility of the structure.

From the peak load of both concretes, we can observe that the lower the temperature is, the larger the peak load is, and the peak load gradually decreases with an increase in the temperature; secondly, the area enclosed by the curve and the horizontal axis reflect the toughness of both concretes to a certain extent. The larger the area, the better the toughness of the concrete is. The sample made with the OPC obviously has a lower toughness with an increase in the temperature, see Figure 13b.

Porosity (BET method)

In order to validate the interpretations of the strength changes in terms of the microstructural modifications, both concrete samples were examined critically using the Brunauer–Emmett–Teller (BET) method. The pore size distribution was derived from the desorption branch by Barrett-Joyner-Halenda (BJH) method. The test used a 7 cm diameter tube for testing as show in Figure 14. The analysis bath temperature was 77.300 K with a thermal correction. The sample mass was 0.5196 g, with a warm free space of 15.1974 cm³, and a measured cold free space of 47.5088 cm³ with an equilibration interval of 10 s with a low-pressure dose. The sample density was 1.000 g·cm^{-3} with automatic degassing.

The results of each graph, see Figure 15, demonstrates the behaviour tendency of the permeability of both concretes (SACC and OPCC) as a function of the relative pressure (P/Po) and quantity adsorbed (cm^3·g^{-1} STP), as well as the Pore width (nm) characteristic of the strength compression and the surface area single point at P/Po [m^2·g^{-1}]. We can effectively observe that as the temperature increased, the quantity adsorbed became higher for both concretes, but more for the OPCC, thus confirming the greater and increasing porosity of the samples, therefore, increasing its fragility to withstand any force applied.

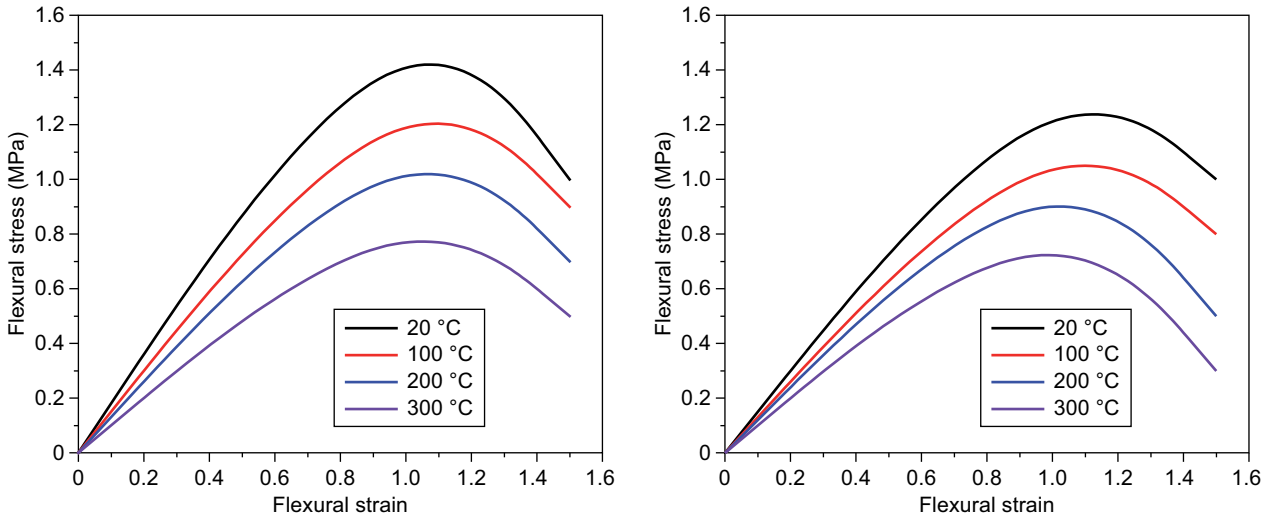

a) SACC b) OPCC

Figure 13. The flexural stress-strain curves of the SACC and the OPCC concretes.

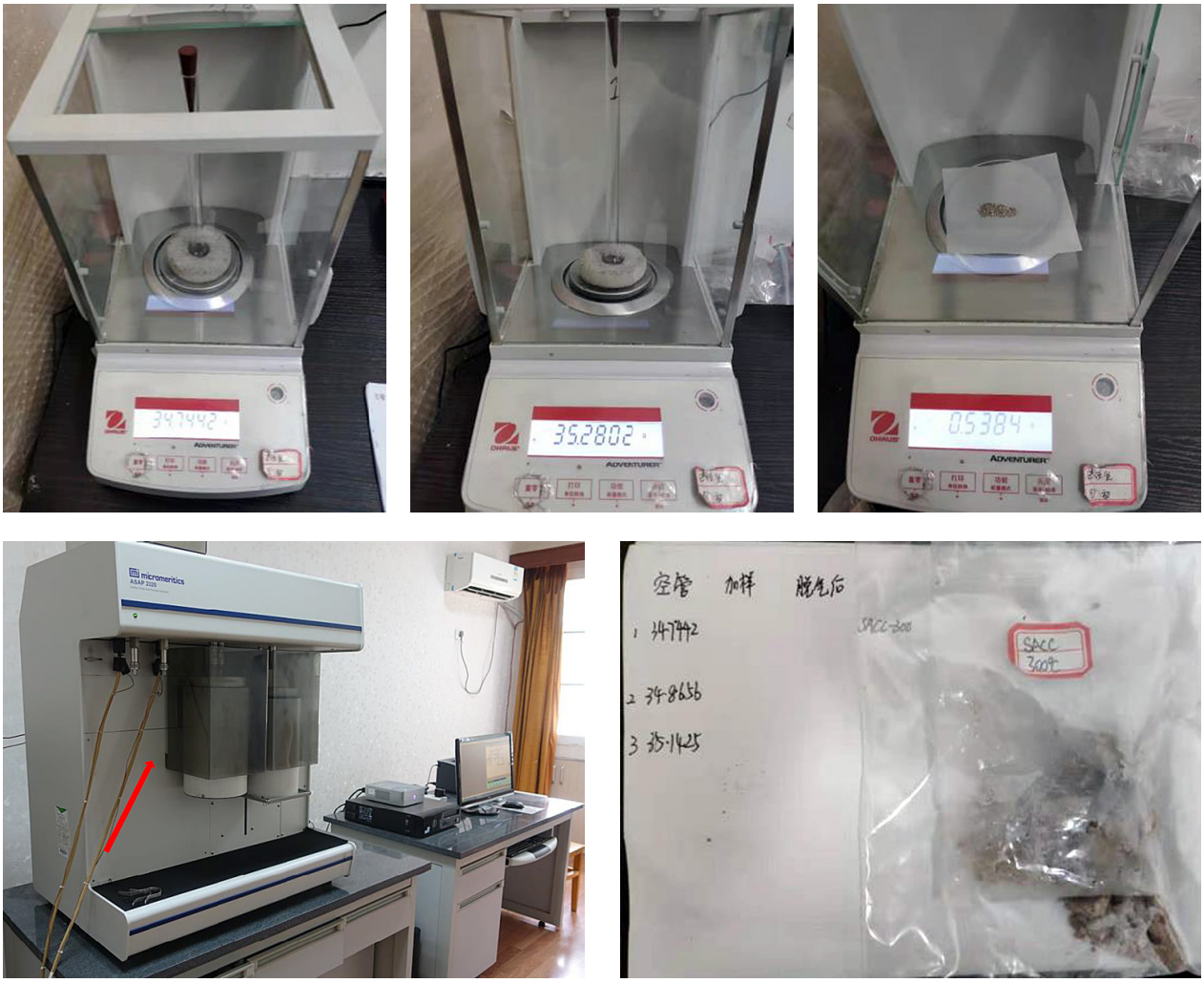

Figure 14. The micromeritic accelerated surface area and porosimetry system testing schematic.

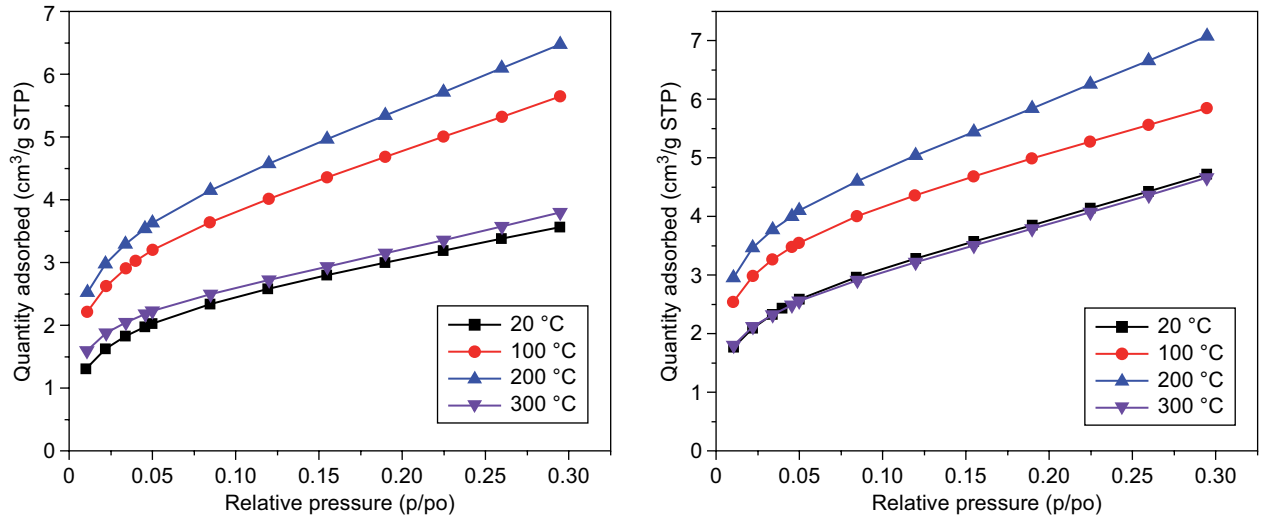

Figure 15. The BET and Isotherm quantity adsorbed vs. the relative pressure. *(Continue on next page)*

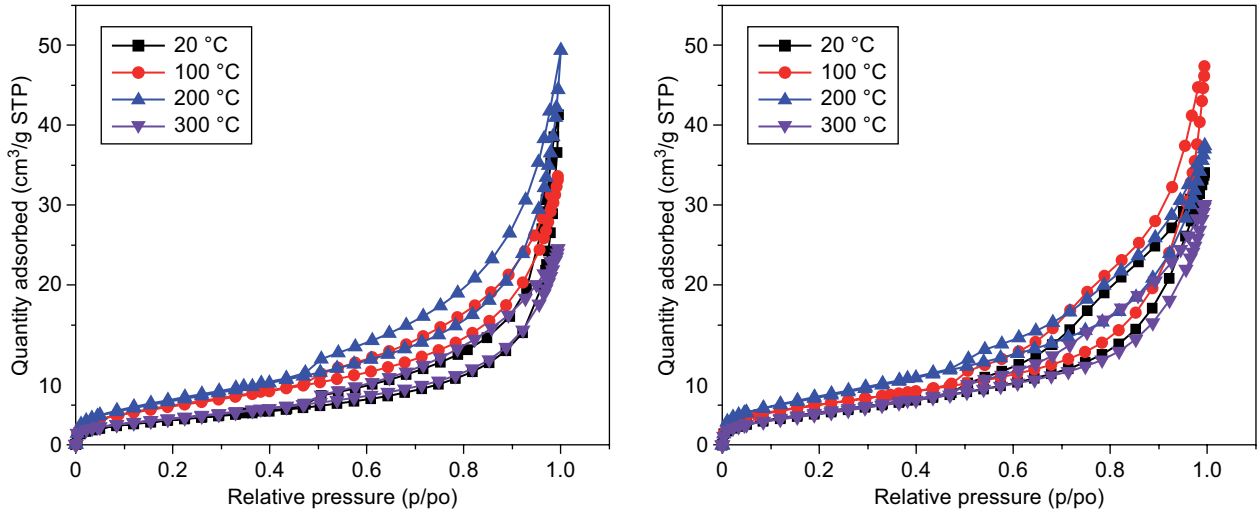

Figure 15. The BET and Isotherm quantity adsorbed vs. the relative pressure.

Taken as a whole, according to the International Union of Pure Applied Chemistry (IUPAC) for the classification of the adsorption isotherm, the curve is a type III curve with an H3 model hysteresis loop, with aggregates (weak mass) of plate-like fragments forming slit-like pores. Characterised by a convexity to the opposite pressure axis. Such isotherms occur when weak gas-solid interactions occur on the non-porous or macro-porous solids, and are uncommon. At 300 °C, for both concretes, there is a downward trend in the quantity adsorbed because some parts of the levy collapse (very porous) because of the fragility of the sample materialised by the aptitude of the levy to withstand during the liquid penetration that will result in a significant reduction of the specific surface area, see Figure 16, therefore, a small adsorbed quantity was recorded. The graphics are presented for both concretes at 20 °C, 100 °C, 200 °C, and 300 °C.

The pore size distribution of the samples heated up to 300 °C of both concretes shows that there are two stages: a mounting peak from 20 °C to 100 °C, then at 200 °C, and then a descending peak at 300 °C, and the distribution of the pores is fairly fine. The pore shape is slit-like, presenting an obvious nano-meter like continuous porous network structure with uniform void distribution 2 ~ 50 nm, with a few micropores (< 2 nm) and macro pores (> 50 nm), which is consistent with the adsorption isotherm. However, the distribution of the pores of the samples heated to 100 °C and 200 °C of both concretes (SACC and OPCC) is broad. These results correlate with the microscopic images of the samples heated to 300 °C. The pore size distribution of both samples heated at 100 °C and 200 °C exhibit an increasing curve until around 14 nm, when the different densification of the concretes made with the SAC occurs. The pore structure analysis indicated that the

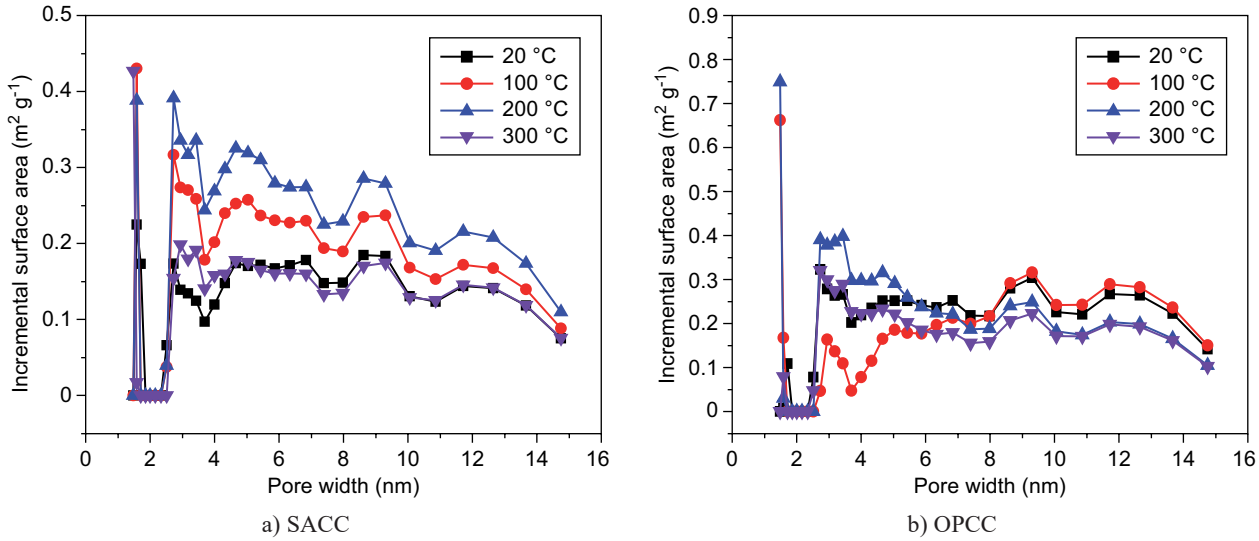

Figure 16. The SACC & OPCC incremental surface area vs. the pore width.

Table 6. The recapitulation of the porosity testing.

Temperatures	20 °C		100 °C		200 °C		300 °C	
	SACC	OPCC	SACC	OPCC	SACC	OPCC	SACC	OPCC
Surface area single point surface area at P/Po [$m^2 \cdot g^{-1}$]	14.49	10.94	17.95	17.33	21.72	19.87	14.31	11.64
BET surface area [$m^2 \cdot g^{-1}$]	14.87	11.32	18.44	17.80	22.16	20.41	14.64	11.87
Pore volume single point adsorption total pore volumeof pores at P/Po [$cm^3 \cdot g^{-1}$]	0.050	0.051	0.066	0.048	0.054	0.063	0.043	0.035
Pore size adsorption average pore diameter (4V/A by BET)	13.57	18.35	14.49	10.94	9.92	12.40	11.96	12.00
BJH Adsorption average pore width (4V/A)	11.29	17.72	14.63	10.19	9.16	11.61	10.41	10.81

pore diameter of both concretes is mostly in the range of being mesoporous (2 and 50 nm). Through the SEM observations, it was found that, for the samples made with the SAC, the compactness was optimal compared with the one made with OPC, which presented an obvious nano-meter like continuous porous network structure with a uniform void distribution for the sample heated at 300 °C.

CONCLUSION

This research work shows the results of the experimental comparative study of the flexural strength behaviour, crack load, compressive strength, mass weight loss, ultrasonic wave testing and flexural strain of the SAC and OPC concrete after being exposed to various high temperatures (e.g., 100, 200 and 300 °C).

- The change in colour allows us to assess the observed heat damage to the concrete samples since it correlates with the starting of the significant loss of strength by the SACC samples. The observation of the SACC and OPCC coming out of the residual electric furnace offers a subjective visual change in colour: yellowish for the samples made with SAC, a sign of a significant loss of strength by the SACC, whereas the one made with OPC maintained up to 80 % of its original colour when heated to 300 °C.
- Initially, the flexural strength of the SACC is 27 % higher than the OPCC showing it to be stronger in terms of the load carrying capacity; decreasing to 35 % for 100 °C, 67 % for 200 °C and 17 % for 300 °C of its initial flexural strength against 26 % for 100 °C, 42 % for 200 °C and 39 % for 300 °C for the OPCC of its initial flexural strength, respectively. A ratio reduction strength of 0.034 for the OPCC against 0.030 for the SACC shows that the OPCC has a better resilient strength, it performed more constantly in decreasing the strength as the temperature increased than the SACC which had a rapid decreasing strength. The compressive strength decreases 39 % for 100 °C, 56 % for 200 °C and 55 % for 300 °C for the SACC against 3 % for 100 °C, 6 % for 200 °C and 20 % for 300 °C for the OPCC, respectively. Both concretes continued to lose strength after being heated and cooled for an extensive period of 7 days, which means that the air cooling did not aid the samples to recover their strength.
- The flexural stress-strain trend in the curves of the SACC under the same temperature and strain conditions, has a higher yield stress as the temperature increases exhibit peak stresses, which decreases rapidly when compare to the OPCC when the temperature is increased, the peak stress of each curve decreases uniformly, and the peak stress and its corresponding strain become smaller. The ultrasonic wave testing and porosity (BET) data agreed with each other on both samples made with the different cements (SAC and OPC). The amplitudes values decreased to 0.96 mV for 100 °C, 0.82 mV for 200 °C, and 0.81 mV for 300 °C and 1.28 mV for100 °C, 1.20 mV for 200 °C, 0.60 mV for 300 °C for the SACC and the OPCC, respectively, that correlated with the trends in the curve appearance of the internal pore sizes where a clear trend in the number of wider cracks increases with the increasing temperature in general.

Disclosing the variations in the homogeneity and density of the SAC and OPC concrete that went through extreme temperatures (e.g., 100, 200 and 300 °C), this research data could contribute to the rebuilding and repairing of construction dilemmas. The SACC mechanical properties exposed to high temperatures are revealed to be fair up to 200 °C. The mechanical properties, such as the flexural strength, porosity, ultrasonic testing and mass weight decrease in value when exposed to high temperatures. The results of this study suggest the dependence of mechanical properties on an ambient, non-heated environment.

Acknowledgements

This work was supported by the National Natural ScienThis work was supported by the National Natural Science Foundation of China (No.51761145023 and 51632003), the Taishan Scholars Program, and the Case-by-Case Project for Top Outstanding Talents of Jinan.

REFERENCES

1. da Costa E. B., Rodríguez E. D., Bernal S. A., Provis J. L., Gobbo L. A., Kirchheim A. P. (2016): Production and hydration of calcium sulfoaluminate-belite cements derived from aluminium anodising sludge. *Construction and Building Materials*, *122*, 373-383. Doi: 10.1016/j.conbuildmat.2016.06.022
2. Colorado H. A., Garcia E., Buchely M. F. (2016). White Ordinary Portland Cement blended with superfine steel dust with high zinc oxide contents. *Construction and Building Materials*, *112*, 816-824.Doi:10.1016/j.conbuildmat.2016.02.201
3. Jaber H. A., Mahdi R. S., Hassan A. K. (2019): Influence of eggshell powder on the Portland cement mortar properties. *Materials Today: Proceedings* 88, 165-171. Doi: 10.1016/j.matpr.2019.09.153
4. Kleib J., Aouad G., Louis G., Zakhour M., Boulos M., Rousselet A., Bulteel D. (2018): The use of calcium sulfoaluminate cement to mitigate the alkali silica reaction in mortars. *Construction and Building Materials*, *184*, 295-303. Doi: 10.1016/j.conbuildmat.2018.06.215
5. Péra J., Ambroise J. (2004): New applications of calcium sulfoaluminate cement. *Cement and Concrete Research 34* (4), 671-676. Doi: 10.1016/j.cemconres.2003.10.019
6. Lu L., Wang S., Cheng X. (2012): Effect of admixture on sulfate resistance of alite-barium calcium sulphoaluminate cement mortar. *Journal of Structural Integrity and Maintenance*, *27*, 237-243. Doi: 10.1016/j.proeng.2011.12.449
7. Lim J. S., Cheah C. B., Ramli M. B. (2019): The setting behavior, mechanical properties and drying shrinkage of ternary blended concrete containing granite quarry dust and processed steel slag aggregate. *Construction and Building Materials*, *215*, 447-461. Doi: 10.1016/j.conbuildmat.2019.04.162
8. Vigneshwaran K., Sodhi G. S., Muthukumar P., Subbiah S. (2019): Concrete based high temperature thermal energy storage system: Experimental and numerical studies. *Energy Conversion and Management*, *198*, 111-905. Doi: 10.1016/j.enconman.2019.111905
9. Kumar R., Bhattacharjee B. (2003): Porosity, pore size distribution and in situ strength of concrete. Cement and Cement *and Concrete Research*, *33*,155-164. Doi: 10.1016/S0008-8846(02)00942-0
10. Duthinh, D. (2017): Structural design for fire: A survey of building codes and standards. *National institute of standards and technology*, *35*, 774-785. Doi: 10.6028/nist.tn.1842
11. Zhang J., Li G., Ye W., Chang Y., Liu Q., Song, Z. (2018): Effects of ordinary Portland cement on the early properties and hydration of calcium sulfoaluminate cement. *Construction and Building Materials*, *186*, 1144-1153. Doi: 10.1016/j.conbuildmat.2018.08.008
12. Li H., Yang K., Guan X. (2019): Properties of sulfoaluminate cement-based grouting materials modified with LiAl-layered double hydroxides in the presence of PCE superplasticizer. *Construction and Building Materials*, *226*, 399-405. Doi: 10.1016/j.conbuildmat.2019.07.210
13. Ferche A. C., Gautam B., Habibi F., Panesar D. K., Sheikh S. A., Vecchio F. J., Orbovic N. (2019): Material, structural and modelling aspects of alkali aggregate reaction in concrete. *Journal of Civil Engineering and Management*, *209*, 87-93. Doi: 10.1016/j.nucengdes.2019.05.019
14. Sephton M. G., Webb J. A. (2019): The role of secondary minerals in remediation of acid mine drainage by Portland cement. *Journal of Hazardous Materials*, *367*, 267-276. Doi: 10.1016/j.jhazmat.2018.12.035
15. Abdelkarim O.I., Ahmed E. A., Mohamed M. H., Benmokraned B. (2019): Flexural strength and serviceability evaluation of concrete beams reinforced with deformed GFRP bars. *Engineering Structures, 186*, 282-296. Doi: 10.1016/j.engstruct.2019.02.024
16. Cheilakou E., Tsopelas N., Anastasopoulos A., Kourousis D., Rychkov D., et al. (2018): Strain monitoring system for steel and concrete structures. *Procedia Structural Integrity*, *10*, 25-32. Doi: 10.1016/j.prostr.2018.09.005
17. Peng F., Xue W. (2018). (2018): Design approach for flexural capacity of concrete T-beams with bonded prestressed and nonprestressed FRP reinforcements. *Composite Structures*, *204*, 333-341. Doi:10.1016/j.compstruct.2018.07.091
18. Coutts D. R., Wang J., Cai J. G. (2018): Monitoring and analysis of results for two strutted deep excavations using vibrating wire strain gauges. *Tunnelling and Underground Space Technology*, *16,* 87-92. Doi:10.1016/S0886-7798(01)00032-3
19. Rao S. K., Sravana P., Rao T. C. (2016): Experimental studies in Ultrasonic Pulse Velocity of roller compacted concrete pavement containing fly ash and M-sand. *International Journal of Pavement Research and Technology*, *9*, 289-301. Doi: 10.1016/j.ijprt.2016.08.003
20. Adesina A., Awoyera P. O., Sivakrishna A., Kumar K. R., Gobinath R. (2019). Phase change materials in concrete: An overview of properties. *Materials Today: Proceedings*, *26*, 233-29. Doi: 10.1016/j.matpr.2019.11.228
21. Güçlüer K. (2019): Investigation of the effects of aggregate textural properties on compressive strength (CS) and ultrasonic pulse velocity (UPV) of concrete. *Journal of Building Engineering*, *27*, 100949. Doi: 10.1016/j.jobe.2019.100949
22. Janků M., Cikrle P., Grošek J., Anton O., Stryk J. (2019): Comparison of infrared thermography, ground-penetrating radar and ultrasonic pulse echo for detecting delamination in concrete bridges. *Construction and Building Materials*, *225*, 1098-1111. Doi: 10.1016/j.conbuildmat.2019.07.320
23. Carmona M., Cortés C. (2014): Analysis of the thermal performance and convection effects in an aluminum holding furnace using CFD. *Applied Thermal Engineering*, *76*, 484-495. Doi: 10.1016/j.applthermaleng.2014.11.044
24. Elias R. S., Yuan M., Wahab M. I. M., Patel N. (2018): Quantifying saving and carbon emissions reduction by upgrading residential furnaces in Canada. *Journal of Cleaner Production*, *211*, 1453-1462. Doi: 10.1016/j.jclepro.2018.11.214
25. Loutas T. H., Panopoulou A., Roulias D., Kostopoulos V. (2012): Intelligent health monitoring of aerospace composite structures based on dynamic strain measurements. *Expert Systems with Applications*, *39*, 8412-8422. Doi: 10.1016/j.eswa.2012.01.179
26. Czarnecki L., Garbacz A., Krystosiak M. (2006): On the ultrasonic assessment of adhesion between polymer coating and concrete substrate. *Cement and Concrete Composites*, *28*, 360-369. Doi: 10.1016/j.cemconcomp.2006.02.017